Pharmacological Research 161 (2020) 105157

Contents lists available at ScienceDirect

Pharmacological Research

journal homepage: www.elsevier.com/locate/yphrs

MAP30 protein from *Momordica charantia* is therapeutic and has synergic activity with cisplatin against ovarian cancer *in vivo* by altering metabolism and inducing ferroptosis

David W Chan [a,*], Mingo MH Yung [a], Yau-Sang Chan [a], Yang Xuan [a], Huijuan Yang [b], Dakang Xu [c], Jin-Biao Zhan [d], Karen KL Chan [a], Tzi-Bun Ng [e], Hextan YS Ngan [a,**]

[a] Department of Obstetrics & Gynaecology, LKS Faculty of Medicine, The University of Hong Kong, Hong Kong Special Administrative Region
[b] Department of Gynecological Oncology, Fudan University Shanghai Cancer Center, Fudan University, Shanghai, 200032, PR China
[c] Faculty of Medical Laboratory Science, Ruijin Hospital, School of Medicine, Shanghai Jiao Tong University, Shanghai, 200030, PR China
[d] Department of Biochemistry, Zhejiang University School of Medicine, 866 Yuhangtang Road, Zijingang Campus, Hangzhou, Zhejiang, 310058, PR China
[e] School of Biomedical Sciences, The Chinese University of Hong Kong, Hong Kong Special Administrative Region

ARTICLE INFO

Keywords:
MAP30
bitter melon
ovarian cancer
chemoresistance
metabolism
ferroptosis

Chemical compounds in this article:
A23187 (PubChem CID: 40486)
AICAR (PubChem CID: 46780289)
BODIPY (PubChem: CID: 25058173)
Cisplatin (PubChem CID: 441203)
Erastin (PubChem CID: 11214940)
Ferrostatin 1 (PubChem CID: 4068248)
NaCl (PubChem CID: 5234)
Phenylmethylsulfonyl fluoride (PMSF) (PubChem CID: 4784)
Propidium iodide (PI) (PubChem CID: 104981)
PVDF (PubChem CID: 3082294)
STO-609 (PubChem CID: 3467590)
Tris-HCl (PubChem CID: 93573)

ABSTRACT

Increasing evidence shows that Traditional Chinese Medicine (TCM) has an obvious appeal for cancer treatment, but there is still a lack of scientific investigation of its underlying molecular mechanisms. Bitter melon or bitter gourd (*Momordica charantia*) is an edible fruit that is commonly consumed, and it is used to cure different diseases in various ancient folk medical practices. We report that a bioactive protein, MAP30, isolated from bitter melon seeds exhibited potent anticancer and anti-chemoresistant effects on ovarian cancer cells. Functional studies revealed that MAP30 inhibited cancer cell migration, cell invasion, and cell proliferation in various ovarian cancer cells but not normal immortalized ovarian epithelial cells. When administered with cisplatin, MAP30 produced a synergistic effect on cisplatin-induced cell cytotoxicity in ovarian cancer cells. When low doses of cisplatin and MAP30 were co-injected intraperitoneally, a remarkable reduction of tumor dissemination and tumor growth was observed in an ovarian cancer ascites mouse model. Notably, blood tests confirmed that MAP30 did not cause any adverse effects on liver and kidney functions in the treated mice. MAP30 activated AMP-activated protein kinase (AMPK) signaling via CaMKKβ and induced cell cycle arrest in the S-phase. MAP30 modulated cell metabolism of ovarian cancer cells via suppression of GLUT-1/-3-mediated glucose uptake, adipogenesis, and lipid droplet formation in tumor development and progression. MAP30 also induced an increase in intracellular Ca^{2+} ion concentration, which triggered ROS-mediated cancer cell death via apoptosis and ferroptosis. Collectively, these findings suggest that natural MAP30 is a non-toxic supplement that may enhance chemotherapeutic outcomes and benefit ovarian cancer patients with peritoneal metastases.

Abbreviations: AICAR, 5-Aminoimidazole-4-carboxamide ribonucleotide; AST, Aspartate aminotransferase; ALT, Alanine aminotransferase; ATCC, American Type Culture Collection; AMPK, AMP-activated protein kinase; BME, Bitter melon extract; Ca^{2+}, Calcium ion; CaMKKβ, Calcium/Calmodulin-Dependent Protein Kinase Beta; ERK, Extracellular signal-regulated kinases; Fer1, Ferrostatin 1; FOXM1, Forkhead box protein M1; GLUT-1/-3, Glucose transporter -1/-3; GPX4, Glutathione Peroxidase 4; HIV, Human immunodeficiency virus; HOSE, Immortalized human ovarian surface epithelium; IC50, The half maximal inhibitory concentration; i.p., Intraperitoneal; LDH, Lactate dehydrogenase; MAP30, Momordica anti-HIV protein; NH_4OAc, Ammonium acetate; OCM, Omental conditioned medium; PI, Propidium iodide; PVDF, Polyvinylidene difluoride; ROS, Reactive oxygen species; SDS-PAGE, Sodium dodecyl sulfate polyacrylamide gel electrophoresis; sgRNA, Single guide RNA; TCM, Traditional Chinese Medicine; xCT, The cystine/glutamate transporter.

* Corresponding author at: Department of Obstetrics and Gynaecology, L747 Laboratory Block, LKS Faculty of Medicine, 21 Sassoon Road, Pokfulam, Hong Kong Special Administrative Region.

** Corresponding author at: Department of Obstetrics and Gynaecology, 6/F Professorial Block, Queen Mary Hospital, Pokfulam, Hong Kong Special Administrative Region.

E-mail addresses: dwchan@hku.hk (D.W. Chan), hysngan@hku.hk (H.Y. Ngan).

https://doi.org/10.1016/j.phrs.2020.105157
Received 27 April 2020; Received in revised form 11 August 2020; Accepted 12 August 2020
Available online 16 August 2020

1. Introduction

Ovarian cancer is one of the most lethal gynecological malignancies worldwide, including China (1). Due to the lack of reliable symptoms and biomarkers during the early stages, most ovarian cancer patients succumb to the advanced-stage disease, which is accompanied by peritoneal metastases and poor prognosis (2). Platinum-based drugs, such as cisplatin, are the most potent anticancer agents commonly used to treat advanced ovarian cancers (3). However, the significant limitations of these drugs include the acquisition of resistance in initially responsive tumors and severe side effects at higher doses. Therefore, the examination of alternative anticancer approaches, such as the use of foods and herbal supplements in combination with current chemotherapy, is urgently needed to improve the treatment efficacy of available drugs. AMP-activated protein kinase (AMPK) is a metabolic energy sensor that governs energy homeostasis in cells (4). We and others recently found that low AMPK activity favored cancer cell growth, and treatment with AMPK activators, such as AICAR or metformin, markedly inhibited cell growth (5–7). Increasing evidence shows that Traditional Chinese medicine (TCM) is an obvious choice for cancer treatment (8), but there is a lack of scientific investigation of its underlying molecular mechanisms. Evidence-based TCM for cancer therapy indicates that TCM targets cancer cells and treats the entire body (9). The bioactive compounds from TCM exert anti-tumor activities via the targeting of multiple levels and signaling pathways. Therefore, TCM may be used as an adjunct cancer therapy. Bitter melon or bitter gourd (*Momordica charantia*) is an edible fruit that is commonly consumed, and it is used to cure different diseases in various ancient folk medical practices (10). Our previous study suggested that bitter melon extract (BME) functioned similarly to a natural AMPK activator in human cancer cell growth suppression and apoptosis induction without toxic effects in normal cells (11). Momordica anti-HIV protein (MAP30) is one of the most bioactive components in BME, and it possesses immunomodulatory, anti-tumor, anti-viral, and anti-human immunodeficiency virus (HIV) activities and inhibits *in vitro* protein synthesis (12). However, the anti-tumorigenic and anti-chemoresistant effects of MAP30 in advanced ovarian cancer cells are not clear.

The present study performed a comprehensive investigation to characterize the effects of natural MAP30 isolated from bitter melon seeds on ovarian cancer cells. We used our established omental conditioned medium (OCM) and the mouse tumor xenograft model and demonstrated that non-toxic MAP30 exhibited potent anticancer and anti-chemoresistant effects on ovarian cancer cells in combination with cisplatin. These findings suggest that MAP30 may be used as a supplement to enhance the treatment outcomes of current platinum-based chemotherapy regimens.

2. Materials & Methods

2.1. Cell lines and human clinical samples

The human ovarian cancer cell line A2780cp was provided by Prof. Benjamin Tsang, University of Ottawa, Canada. HEY and HEYA8 human ovarian carcinoma cells were provided by Prof. AWS Wong, School of Biological Sciences, University of Hong Kong. ES2 human epithelial ovarian cancer cells and the human embryonic kidney cell line HEK293 were purchased from American Type Culture Collection (ATCC, Manassas, VA, USA). Another human ovarian cancer cell line; OVCA433 and SKOV3, as well as two immortalized human ovarian surface epithelium (HOSE) cell lines; HOSE11-12 and HOSE96-9-18, were provided by Professor G. S. W. Tsao, School of Biomedical Sciences, The University of Hong Kong. A pair of wildtype (WT) and mutant (R531G) AMPKγ2 isogenic HEK293 cells were provided by Prof. DG Hardie, Dundee University, UK. All cell lines were *mycoplasma* free. Human omental tissues were collected from surgeries performed at Queen Mary Hospital with prior approval of the Institutional Review Board of The University of Hong Kong/Hospital Authority Hong Kong West Cluster (HKU/HA HKW IRS) (IRS Reference Number: UW 11-298).

2.2. Purification of natural MAP30 from bitter melon dried seeds

Natural MAP30 was isolated from dried seeds of Chinese bitter melon (bitter gourd). The complete isolation and purification protocols are deposited as Supplementary Information. Further details are described in Supplementary Information.

2.3. CRISPR/Cas9-mediated gene knockout

Knockout of the AMPK α1 and α2 genes was performed via the transfection of pL-CRISPR.EFS.GFP plasmids carrying sgRNA oligonucleotides of AMPKα1 and α2 (provided by Prof. DG Hardie, Dundee University, UK). After transfection, puromycin was used for screening. Western blot analysis was used to detect positive gene knockout clones of AMPKα1 and α2.

2.4. Western blot analysis

Protein lysates were isolated from cells using cell lysis buffer (Cell Signaling Technology, Danvers, MA, USA) containing a protease inhibitor cocktail (Roche, Basel, Switzerland) and phenylmethylsulfonyl fluoride (Sigma-Aldrich Corp., St. Louis, MO, USA). Proteins were separated using 10% SDS-PAGE before transfer to polyvinylidene difluoride (PVDF) membranes. Immunodetection was performed using an enhanced chemiluminescence reagent solution and visualized on X-ray film or imaged by an Odyssey® CLx Imaging and analyzed with Image StudioTM Software (Li-Cor Biosciences). (LI-COR Biosciences, Lincoln, Nebraska, USA). The list of antibodies used in this study is attached in the Supplementary Information.

2.5. Cell cycle and cell apoptosis analyses

Ovarian cancer cells were stained with 250 μL of 50 μg/mL propidium iodide (PI) (P1304MP, Invitrogen) in PBS for 15 min in the dark. Flow cytometry was performed using a BD FACSCantoTM II System (BD Biosciences, San Jose, CA, USA). The proportion of cells in each phase of the cell cycle was analyzed using Modfit LT software (Verity Software House, Topsham, ME, USA). To detect cell apoptosis, the treated cells were stained using the Annexin V FITC Apoptosis Detection Kit TDS, according to the manufacturer's protocol (BD Biosciences). The percentage of apoptotic cells was analyzed using the BD FACSVerse™ System (BD Biosciences) after flow cytometry. To examine the levels of activated caspase-3 and -7 in ovarian cancer cells after MAP30 treatment, the treated cells in 48-well microplates (CLS3548, Corning, NY, USA) were analyzed using the CellEvent™ Caspase-3/7 Green Detection Reagent (C10423, Invitrogen), according to manufacturer's protocol.

2.6. Lipid peroxidation assay and determination of GSH/GSSG activity

To evaluate lipid peroxidation or ferropotosis of ovarian cancer cells co-treated with MAP30 (40 μg/mL), and Erastin (5 μM) (B1524, APExBIO Technology LLC., Boston, MA, USA) alone, or the ferroptosis inhibitor ferrostatin-1 (Fer-1) (10 μM) (SML0583, Sigma-Aldrich, St. Louis, MI, USA) in combination with MAP30 (40 μg/mL) for 24 h, C11 BODIPY 581/591 C11 dye (Lipid Peroxidation Sensor) (2.5 μM) (D3861, ThermoFisher Scientific, Waltham, MA USA), were used (13). Flow cytometry analysis was performed using a BD FACSLyric™ flow cytometry system (BD Biosciences, San Jose, CA, USA), and at least 10,000 cells were analyzed per cell sample. The oxidation of C11 BODIPY 581/591 was shown by the rise of green fluorescent intensity (which indicates oxidized probe) in the FITC channel. The data were analyzed using FlowJo Version 7.6 software. For confocal imaging experiments, the treated ovarian cancer cells of each experimental group were

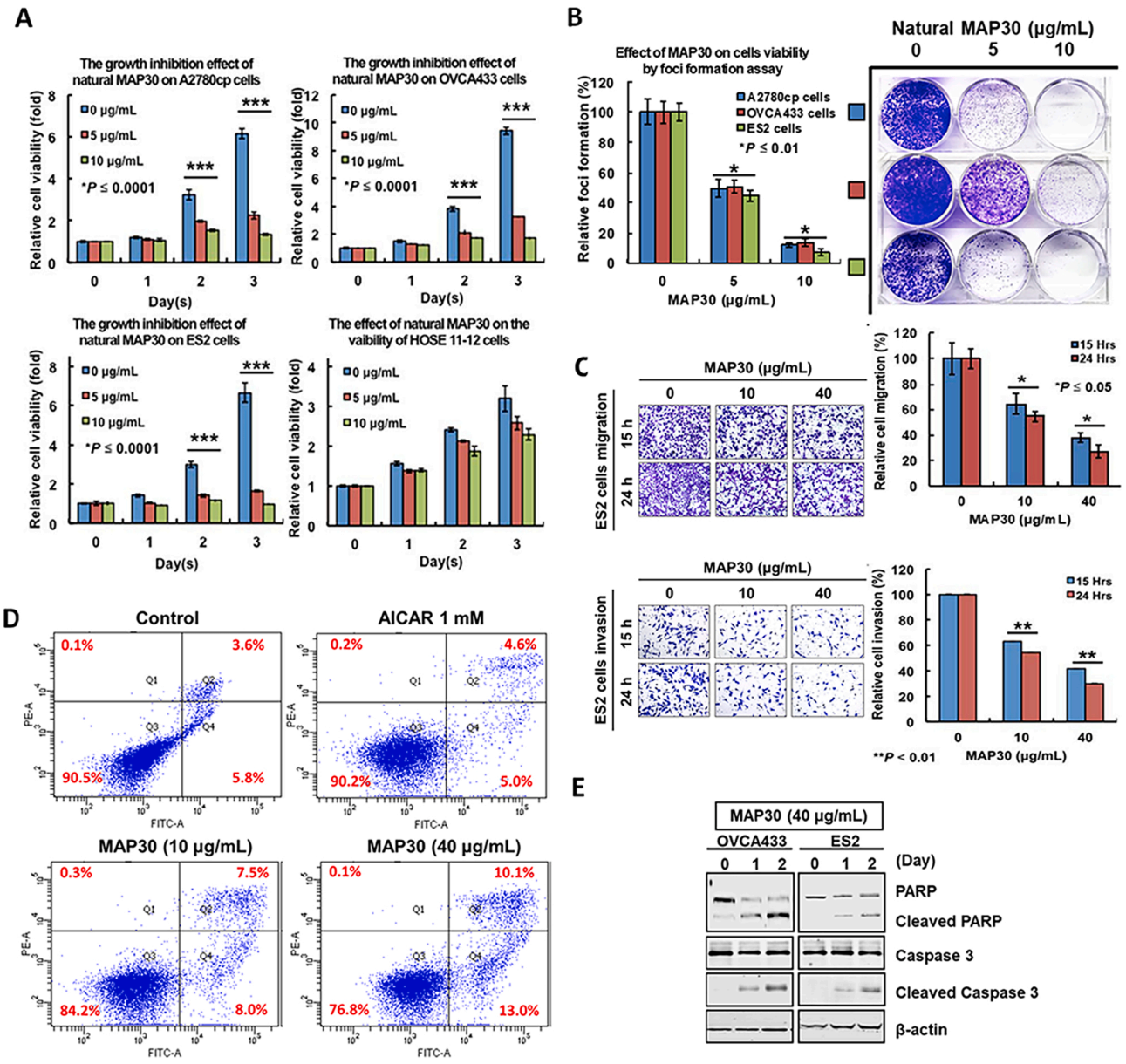

Fig. 1. MAP30 is a main component of BME and functions as a natural AMPK activator. (A) XTT cell proliferation assay showed the inhibition of cell proliferation of ovarian cancer cells dose-dependently, but there was no effect on HOSE11-12. (**B**) Focus formation assay demonstrated that MAP30 reduced the number of foci formed in ovarian cancer cells (A2780cp, OVCA433, and ES2) at 5 and 10 μg/mL, respectively, for one week. (C) Transwell migration assay showed that ES2 cells treated with MAP30 (10 and 40 μg/mL) exhibited a significant reduction in the number of cells penetrating through the membrane in a dose-dependent manner compared with untreated controls (*upper*). ES2 cells treated with MAP30 (10 and 40 μg/mL) showed less invaded cells through the matrigel compared with the control (*lower*). (D) Flow cytometry analyzed Annexin-V and Propidium iodide (PI) positive staining (apoptotic cells) in OVCA433 cells treated by MAP30 (10 and 40 μg/mL) and AICAR (1 mM). (E) Western blot analysis showed cleavage of caspase3 and PARP (=cell apoptosis) in OVCA433 ad ES2 cells treated by MAP30 (40 μg/mL) for 24-48 h. All bar charts are expressed as mean ± SEM. *P < 0.05, **P < 0 .01, ***P < 0 .001 (compared with the control group).

examined and imaged using a confocal imaging system (Carl Zeiss LSM 800). Three independent biological replicates were performed for each condition following the manufacturer's protocols.

Changes in the GSH/GSSG ratios of ovarian cancer cells following co-treatment of MAP30 and/or Erastin were detected using the GSH/GSSG Ratio Detection Assay Kit II (Fluorometric - Green) (ab205811, Abcam, Cambridge, MA, USA) according to the manufacturer's instructions.

2.7. Fluo-4 NW calcium assay

To evaluate the amount of intracellular calcium, the Fluo-4 NW Calcium Assay kit (F36206, Thermo) was used following the manufacturer's protocol.

2.8. Determination of ATP level and Reactive Oxygen Species (ROS) production

The amount of ATP within the ovarian cancer cells was evaluated using the Luminescent ATP Detection Assay Kit (ab113849, Abcam). Cellular ROS production was assessed using the DCFDA - Cellular ROS Assay (ab113851, Abcam) according to the manufacturer's protocol.

2.9. Glucose uptake and lactate production

The level of glucose uptake in ovarian cancer cells was measured using the Glucose Uptake Assay Kit (Colorimetric) (ab136955, Abcam). To measure lactate production in and secreted from ovarian cancer cells,

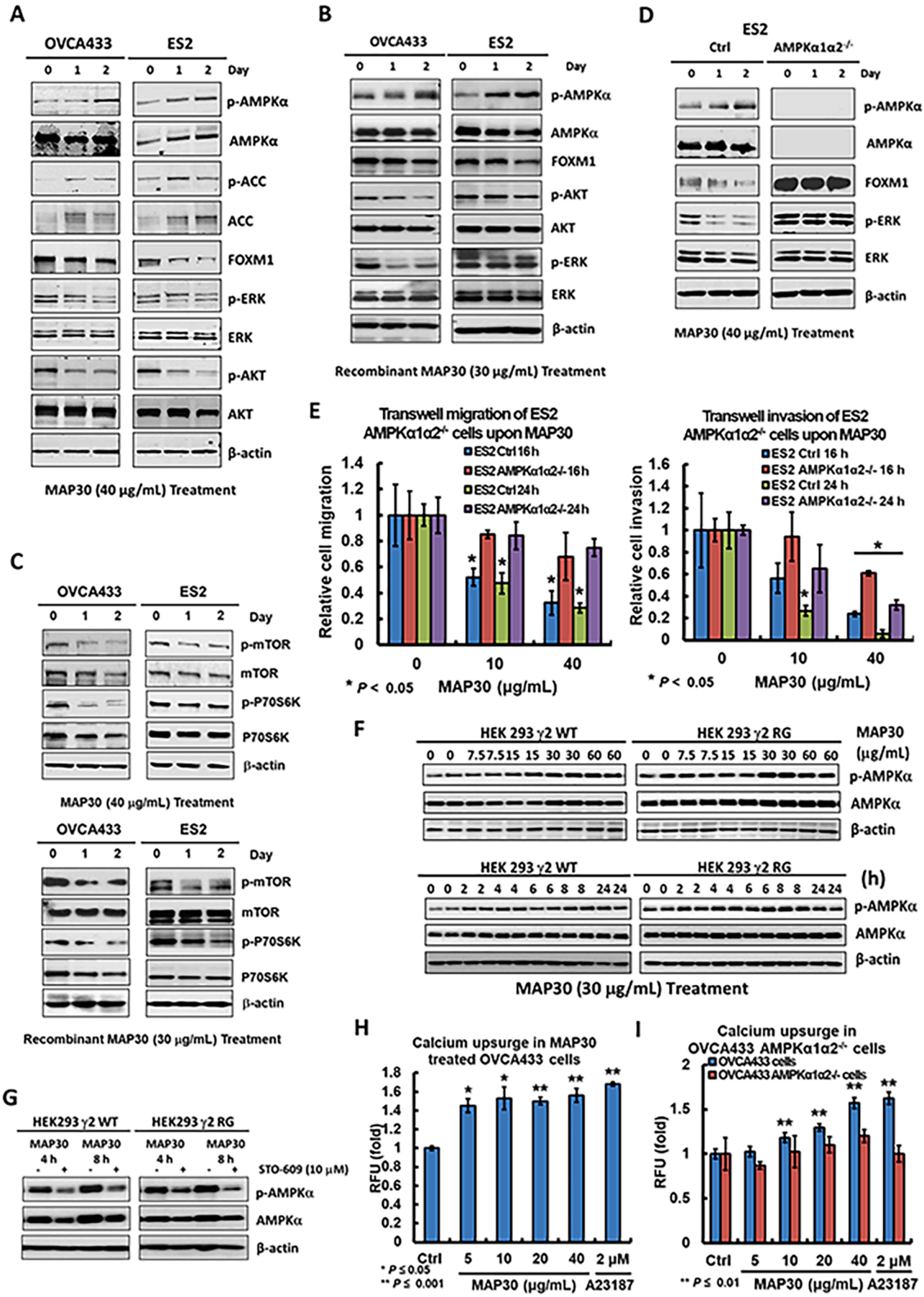
A
OVCA433
ES2
Day
p-AMPKα
AMPKα
p-ACC
ACC
FOXM1
p-ERK
ERK
p-AKT
AKT
β-actin
MAP30 (40 μg/mL) Treatment
B
OVCA433
ES2
p-AMPKα
AMPKα
FOXM1
p-AKT
AKT
p-ERK
ERK
β-actin
Recombinant MAP30 (30 μg/mL) Treatment
D
ES2
Ctrl
AMPKα1α2-/-
p-AMPKα
AMPKα
FOXM1
p-ERK
ERK
β-actin
MAP30 (40 μg/mL) Treatment
C
OVCA433
ES2
p-mTOR
mTOR
p-P70S6K
P70S6K
β-actin
MAP30 (40 μg/mL) Treatment
Recombinant MAP30 (30 μg/mL) Treatment
E
Transwell migration of ES2 AMPKα1α2-/- cells upon MAP30
ES2 Ctrl 16h
ES2 AMPKα1α2-/- 16h
ES2 Ctrl 24h
ES2 AMPKα1α2-/- 24h
Relative cell migration
* P < 0.05
MAP30 (μg/mL)
Transwell invasion of ES2 AMPKα1α2-/- cells upon MAP30
ES2 Ctrl 16 h
ES2 AMPKα1α2-/- 16 h
ES2 Ctrl 24 h
ES2 AMPKα1α2-/- 24 h
Relative cell invasion
* P < 0.05
MAP30 (μg/mL)
F
HEK 293 γ2 WT
HEK 293 γ2 RG
MAP30 (μg/mL)
p-AMPKα
AMPKα
β-actin
(h)
MAP30 (30 μg/mL) Treatment
G
HEK293 γ2 WT
HEK293 γ2 RG
MAP30 4 h
MAP30 8 h
STO-609 (10 μM)
p-AMPKα
AMPKα
β-actin
H
Calcium upsurge in MAP30 treated OVCA433 cells
RFU (fold)
* P ≤ 0.05
** P ≤ 0.001
Ctrl
MAP30 (μg/mL)
A23187
I
Calcium upsurge in OVCA433 AMPKα1α2-/- cells
OVCA433 cells
OVCA433 AMPKα1α2-/- cells
RFU (fold)
** P ≤ 0.01
Ctrl
MAP30 (μg/mL)
A23187

Fig. 2. MAP30 functions as a natural CaMKKβ/AMPK activator. Western blot analysis showed that the effect of recombinant MAP30 (30 μg/mL) (A) and (B) natural MAP30 (40 μg/mL) on AMPK and its downstream targets, FOXM1 and AKT activities in OVCA433 and ES2 cells. (C) Western blot analysis showed the suppressive effects of recombinant MAP30 (30 μg/mL) and natural MAP30 (40 μg/mL) on mTOR signaling activities in OVCA433 and ES2 cells. (D) Western blot analysis showed the effect of natural MAP30 (40 μg/mL) on AKT/ERK/FOXM1 signaling in OVCA433, ES2, and AMPKα1α2-/- ES2 cells. (E) The transwell cell migration (*upper*) and invasion assays (*lower*) showed the effect of natural MAP30 with various doses (0, 10, and 40 μg/mL) on the cell migratory and invasive capacities of AMPKα1α2-/- ES2 cells as compared with the negative controls (Ctrl) for 16-24 h. (F) An isogenic wildtype (WT) and mutant (RG) HEK293γ2 cell lines showed that MAP30 induced phosphorylation of AMPK in both cell lines in a dose- and time-dependent manner. (G) Western blot analysis showed that co-treatment of CaMKKβ inhibitor, STO-609 (10μM), could abolish the phosphorylation of AMPK induced by MAP30 (40 μg/mL) in both cell lines. (H) Concentration-dependent escalation of cellular calcium in OVCA433 cells treated with MAP30 (5, 10, 20, and 40 μg/mL) for 24 h examined using Fluo-4 NW calcium assay with the treatment of calcium ionophore A23187 (2 μM) as the positive control. (I) The MAP30-mediated concentration-dependent escalation of cellular calcium in OVCA433 AMPKα1α2-/- cells was significantly hampered upon knockout of AMPKα1α2-/- compared with control cells (Ctrl) treated with MAP30 (5, 10, 20 and 40 μg/mL) for 24 h. All bar charts are expressed as mean ± SEM. *P < 0.05, **P < 0 .01, ***P < 0 .001 (compared with the control group).

the L-Lactate Assay Kit (Colorimetric) (ab65331, Abcam) was used according to the manufacturer's protocol.

2.10. Determination of hexokinase and lactate dehydrogenase (LDH) activities

Hexokinase activity was measured using the Hexokinase Activity Assay kit (Colorimetric) (ab136957, Abcam), and LDH activity was measured using the LDH Assay Kit (Colorimetric) (ab102526, Abcam) according to the manufacturer's instructions.

2.11. Targeted metabolite relative quantitation of fatty acids

Targeted metabolite analyses in ascites were performed using gas chromatography-mass spectrometry (GC-MS) at the LKS Faculty of Medicine, Proteomics, and Metabolomics Core Facility (CPOS - PM Core), The University of Hong Kong (HKU). GC/MS chromatograms were acquired in SCAN and SIM mode using an Agilent 7890B GC-Agilent 7010 Triple Quadrapole Mass Spectrometer system. Data analyses were performed using the Agilent MassHunter Workstation Quantitative Analysis Software (CPOS - PM Core, HKU).

2.12. Cell proliferation and focus formation assays

Cell proliferation was evaluated using an XTT cell proliferation kit (Roche, Basel, Switzerland). For the focus formation assays, approximately 1000 cells were cultured in each well of a six-well plate and incubated with different treatments. Colonies were stained with crystal violet and counted.

2.13. CellTiter-Glo® 3D cell viability assay

Ovarian cancer cells were suspended in culture medium containing 2% Geltrex™ Matrix (Gibco BRL, Gaithersburg, MD, USA) and seeded on Nunclon™ Sphera™ 96U-microplates (Thermo Fisher Scientific) with a super low cell attachment surface at a density of approximately 1000 cells/well in triplicate. Cells were subsequently allowed to grow for one week before treatment with each drug (MAP30 and cisplatin) alone at serially diluted concentrations or in combination at a fixed molar ratio for three days. After the drug treatments, viable cells were detected using the CellTiter-Glo® 3D cell viability assay according to the manufacturer's protocols (Promega Corporation, Madison, WI, USA). The IC50 value of each drug was determined using nonlinear regression, and drug synergy was determined using the Combenefit algorithm (14).

2.14. Matrigel cell migration and invasion assays

Cell migratory and invasive abilities were examined using Transwell cell migration and invasion kits (Corning, NY, USA) according to the manufacturer's instructions. The migrated/invaded cells were stained and counted using microscopy.

2.15. In vivo tumorigenicity assay

To study the effect of MAP30 on tumor growth *in vivo*, 2×10^6 ES2 ovarian cancer cells were injected intraperitoneally (*i.p.*) into four-week-old BALB/cAnN-nu female nude mice in groups of five. When palpable tumors were formed in approximately one week, the experimental group was treated once every 2-days via injection of MAP30 (250 μg/kg). The control group was injected *i.p.* with only PBS. Fluorescence Stereomicroscopy (Nikon, Japan) was used to capture fluorescent and bright-field images of tumor nodules spreading in the murine intraperitoneal cavity. The entire animal study was performed according to guidelines approved by The Committee on the Use of Live Animals in Teaching and Research of The University of Hong Kong (CULATR number: 3817-15).

2.16. Data analysis

All experiments were repeated at least three independent times unless otherwise stated. Values are presented as means ± SEM, and a 2-tailed Student's *t*-test was used for comparisons. Fisher's exact test (for parametric data) and the Mann–Whitney test (for non-parametric data) were used, and $P \leq 0.05$ was considered statistically significant.

3. Results

3.1. MAP30 is a main component of bitter melon extract (BME)

Our previous study reported that BME was a natural AMPK activator that suppressed ovarian cancer cell growth, cell migration, and invasion (11). We also observed that BME from different sources activated AMPK to various extents, which suggests a dose-dependent effect of MAP30 (11). We used a monoclonal MAP30 antibody and demonstrated that the amount of MAP30 in Thailand (Thai) BME was the highest (~12 ng/μL), followed by Chinese BME (~ 9.6 ng/μL), and Taiwanese (TW) BME (6 ng/μL) (Supplementary Fig. S1A & S1B), suggesting that the different amounts of MAP30 from three cultivars of bitter melon were entirely consistent with their capacities to activate AMPK in ovarian cancer cells.

Functional studies showed that MAP30 suppressed the cell viability of ovarian cancer cells (A2780cp, OVCA433, and ES2) from 40% to 80% in a dose-dependent manner compared to controls using an XTT cell proliferation assay (Fig. 1A). Notably, the cell proliferation of immortalized human ovarian surface epithelial (HOSE11-12) cells was not significantly inhibited (Fig. 1A). The foci formation assay demonstrated that the number of colonies was markedly reduced from 50% to 90% in ovarian cancer cells (A2780cp, OVCA433, and ES2) following treatment with MAP30 (5 and 10 μg/mL) compared to controls (Fig. 1B). To test whether MAP30 inhibited ovarian cancer cell migration and invasion, ES2 ovarian cancer cells were treated with MAP30 (15 and 40 μg/mL) for 15 and 24 h and subjected to Transwell cell migration/invasion assays. Quantitative analyses showed that 15 and 24 h of MAP30 (15 and 40 μg/mL) treatment reduced the cell migration and cell invasion capacities of ES2 cells by 40-70% in a dose- and time-dependent manner (Fig. 1C). These tumor-suppressive effects were also found in ovarian

cancer cells treated with BME (11). Based on the functional similarities and the MAP30 content-response of BME in ovarian cancer cells, MAP30 is the major bioactive component of BME. MAP30 exhibited selective cytotoxicity and inhibition of ovarian cancer cells, while having no cytotoxicity on normal ovarian epithelial cells.

3.2. MAP30 triggers cell cycle arrest and cell apoptosis in ovarian cancer cells

To delineate the underlying molecular mechanisms of MAP30 inhibition of tumor growth, we investigated the effect of MAP30 on cell cycle progression of ovarian cancer cells using flow cytometry analysis of DNA content. Cell cycle analysis showed that MAP30 caused a notable arrest in S-phase with highly variable levels in various ovarian cancer cells, which was different than the AICAR-induced G1-phase cell cycle arrest (Supplementary Fig. S2). MAP30 is a main component of BME, and it may share similar functional effects with BME on AMPK-mediated cell growth arrest and apoptosis (11,15). Therefore, we examined whether MAP30 functioned like other AMPK activators, such as AICAR, in inducing apoptosis of ovarian cancer cells. OVCA433 ovarian cancer cells treated with MAP30 (10 and 40 μg/mL, 24 h) exhibited a 2-3-fold dose-dependent increase in cell apoptotic rate compared to the negative control (Fig. 1D). The CellEvent™ Caspase-3/-7 Green Detection assay revealed that MAP30 induced mitochondria-mediated caspase activation in ES2 cells following co-treatment with MAP30 and cisplatin (Supplementary Fig. S3). Western blot analysis further confirmed that treatment with MAP30 (40 μg/mL) increased the cleavage of PARP and caspase-3 activity in OVCA433 and ES2 cells (Fig. 1E). These results indicated that MAP30 induced cell cycle S-phase arrest and cell apoptosis in ovarian cancer cells.

3.3. MAP30 functions as a natural AMPK activator

Our previous studies showed that BME was a natural AMPK activator that significantly inhibited the oncogenic capacities of ovarian and cervical cancers via suppression of the AKT/ERK/FOXM1 and AKT/FOXO3a/FOXM1 signaling pathways, respectively (11,16). The present study compared the functional differences between natural MAP30 (isolated from dried bitter melon seeds) and recombinant MAP30 protein (produced by *Escherichia coli)*. Western blot analysis indicated that the natural MAP30 protein (40 μg/mL**)** and recombinant MAP30 protein (30 μg/mL**)** remarkably increased the phosphorylation of AMPK at Thr172 and ACC at Ser79 but reduced the level of FOXM1 and the phosphorylation of AKT (Ser473) and ERK in a time-dependent manner (Fig. 2A & 2B). Given that both recombinant MAP30 (30 μg/mL**)** and natural MAP30 (40 mg/mL) could activate AMPK, they were also shown to suppress another AMPK downstream target mTOR signaling activities in ovarian cancer cells (Fig. 2C). This finding confirmed that natural and recombinant MAP30 exhibited anticancer effects on ovarian cancer cells via negative regulation of the AKT/ERK/FOXM1 and mTOR signaling cascades. Notably, the effects of these proteins were consistent with the functional impact of BME on ovarian and cervical cancer cells (16). To further confirm the negative regulation of the AKT/ERK/FOXM1 signaling cascade and its associated oncogenic properties, we used the CRISPR/Cas9 gene knockout system to delete AMPK-α1 and -α2 (*AMPKα1α2-/-*) in ovarian cancer cells. The results confirmed that the complete depletion of AMPK-α1 and -α2 (*AMPKα1α2-/-*) significantly attenuated the MAP30-mediated suppression of the AKT/ERK/FOXM1 signaling cascade (Fig. 2D) and produced an approximately 2-fold reduction of cell migration and invasion capacities in ovarian cancer cells (Fig. 2E). These results indicate that the suppressive effect of MAP30 occurred via an AMPK-dependent manner.

Unlike most pharmaceutical AMPK activators, MAP30 functioned similarly to BME because both factors increased the phosphorylation of AMPK in WT and R531G AMPKγ2 isogenic HEK293 cells in a dose- and time-dependent manner (Fig. 2F). These results indicate that MAP30-mediated AMPK activation may involve an AMP-independent mechanism. Treatment with the CaMKKβ inhibitor STO-609 (10 μM) significantly impaired the phosphorylation of AMPK in response to MAP30 in WT and R531 G HEK293 cells (Fig. 2G). To further confirm the calcium-dependent manner of MAP30-induced AMPK activation in ovarian cancer cells, the Fluo-4 NW calcium assay was used. The results showed that the cellular level of calcium ions (Ca^{2+}) in OVCA433 cells increased dose-dependently compared to the control with MAP30 co-treatment (Fig. 2H). In contrast, CRISPR/Cas9-mediated gene knockout of AMPKα1 and α2 (*AMPKα1α2-/-*) reduced the increase in intracellular Ca^{2+} (Fig. 2I), which confirmed the pivotal role of CaMKKβ in MAP30-mediated AMPK activation.

Taken together, these data support our hypothesis that MAP30 is a main component of BME that activates AMPK and suppresses AKT/ERK/FOXM1 and mTOR pathways, as well as the associated cell growth, cell migration/invasion of ovarian cancer cells via a CaMKKβ pathway.

3.4. MAP30 induces ferroptosis in ovarian cancer cells

MAP30 produced an increase in intracellular Ca^{2+} in ovarian cancer cells (Fig. 2G), and an influx of Ca^{2+} may increase cytosolic oxidative stress and mitochondrial dysfunction (17). Excessive cytosolic reactive oxygen species (ROS) may produce lipid peroxidation and ferroptosis, which is an alternative form of programmed cell death (18). To investigate whether MAP30 induced ferroptosis, we examined whether MAP30 enhanced ROS production in ovarian cancer cells. We compared MAP30 to the ferroptosis activator Erastin and observed that MAP30 dose-dependently increased intracellular ROS production in ovarian cancer cells (Fig. 3A). Notably, MAP30 induced less ROS production in AMPKα1α2-/- ovarian cancer cells (Fig. 3A). A reduced ratio of glutathione and oxidized glutathione (GSH/GSSG) is a central cellular anti-oxidant system to prevent oxidative damage (19). To investigate whether MAP30 reduced the GSH/GSSG ratio, like Erastin, during the increase in ROS (20), we measured the GSH/GSSG ratio in ovarian cancer cells co-treated with MAP30 and Erastin. MAP30 significantly reduced the GSH/GSSG ratio in a dose-dependent manner and showed an inverse correlation with the ROS level (Fig. 3B). The effect of MAP30 on the GSH/GSSG ratio was diminished in AMPKα1α2-/- ovarian cancer cells, but the effects of Erastin were not different (Fig. 3B). Previous studies suggested that Erastin blocked cellular cysteine uptake via inhibition of the cystine/glutamate antiporter (xCT) and glutathione peroxidase 4 (GPX4), and GSH depletion induced lipid peroxidation and ferroptosis (13,21). Therefore, we compared the effect of MAP30 on GPX4 to Erastin. Western blot analysis showed that MAP30 reduced GPX4 protein similarly to Erastin in a dose-dependent manner in wild-type and AMPKα1α2-/- ovarian cancer cells (20). By using BODIPY™ 581/591 C11 as lipid peroxidation probe, we confirmed that MAP30 induced lipid peroxidation in ovarian cancer cells, and a potent inhibitor of ferroptosis, ferrostatin-1 (Fer-1), inhibited this effect (Fig. 3D & 3E). Because MAP30 had a smaller impact on ROS production and GSH/GSSG ratio depletion in AMPKα1α2-/- ovarian cancer cells, we investigated the MAP30-mediated lipid peroxidation in these cells. Flow cytometry analysis revealed that MAP30 remarkably induced lipid peroxidation, which was counteracted by Fer-1 in ovarian cancer cells (Fig. 3F). However, MAP30 only slightly induced lipid peroxidation in AMPKα1α2-/- ovarian cancer cells (Fig. 3F). These findings confirmed that MAP30 was a ferroptosis inducer in ovarian cancer cells. However, the mechanism of the deletion of AMPK activity reduced the efficiency of MAP30 in the induction of ferroptosis remains unclear. Further investigation is warranted to elucidate the functional role of AMPK in MAP30-induced ferroptosis.

3.5. MAP30 inhibits tumor growth in vivo without producing adverse effects

The highly metastatic human ovarian cancer cell line ES2 labeled

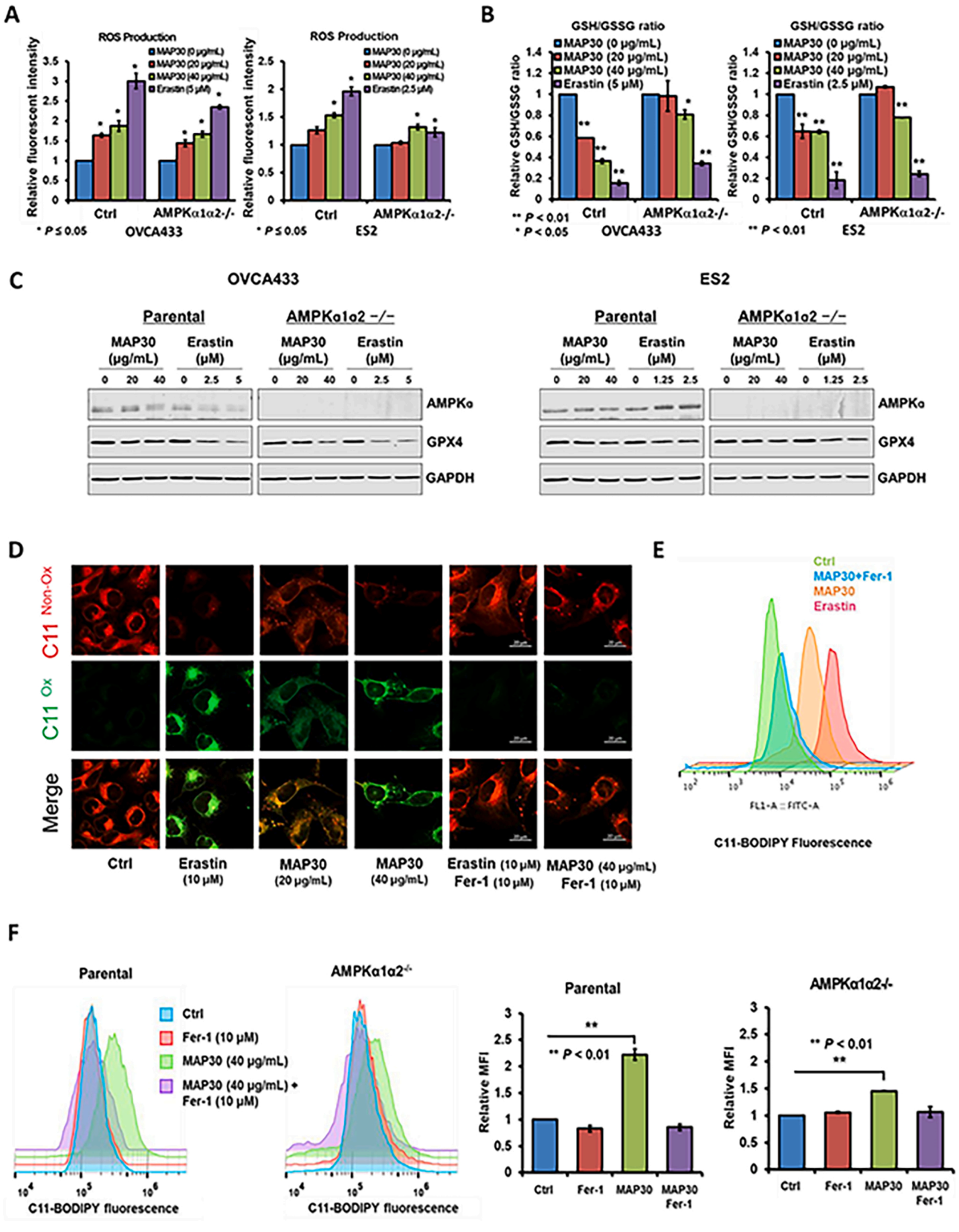

(caption on next page)

Fig. 3. MAP30 induces ferroptosis in ovarian cancer cells. (A) Cellular ROS detection in term of the DCFDA fluorescence intensity was measured by microplate format in OVCA433 and ES2 parental (Ctrl) and AMPKα1α2-/- cells treated with MAP30 (20 and 40 μg/mL) and Erastin (5 and 2.5 μM) for 24 h. (B) Cellular GSH/GSSG ratio detection was measured by fluorometric microplate format in OVCA433 and ES2 cells. Both OVCA433 and ES2 parental (Ctrl) and AMPKα1α2-/- cells co-treated with MAP30 (20 and 40 μg/mL) and Erastin (5 μM on OVCA433 cells and 2.5 μM on ES2 cells) for 24 h showed the reduction of GSH/GSSG ratio. (C) Western blot analysis revealed MAP30 possesses a similar inhibitory effect of Erastin on GPX4 in wildtype and AMPKα1α2-/- OVCA433 and ES2 cells. The treatment time for MAP30 and Erastin was 24 h in various doses. GAPDH was used as the internal control. (D) Confocal imaging showed the lipid peroxidation activity (Green) using C11 BODIPY 581/591 (C11) (ThermoFisher) in OVCA433 cells after treatment of Erastin (10μM), MAP30 (20 and 40 μg/mL) and the combination of Fer-1 (10 μM) with either Erastin (10μM) or MAP30 (40 μg/mL) for 24 h. PBS was used for negative control (Ctrl). $C11^{Non\text{-}ox}$ = non oxidized C11 (Red), $C11^{Ox}$ = oxidized C11 (Green). (Scale bar = 20 μm). (E) Flow cytometry analysis of OVCA433 cells treated with Erastin (10μM) (Red), MAP30 (40 μg/mL) (Orange), and Fer-1 (10 μM) + MAP30 (40 μg/mL) (Blue) for 24 h. PBS was used for negative control (Ctrl) (Green) and stained with C-11 BODIPY (ThermoFisher). (F) Flow cytometry analysis showed MAP30 (40 μg/mL, 24 h) induced stronger effect on lipid peroxidation activity in AMPK wildtype than $AMPK\alpha1\alpha2^{-/-}$ OVCA433 cells. Ferrostatin-1 (Fer-1) (10 μM, 24 h) was treated as a ferroptosis inhibitor (*left*). Bar charts displayed the relative median fluorescence intensity of control and treatment groups (MAP30 and/ or Fer-1) analyzed by flow cytometry (*right*). All bar charts are expressed as mean ± SEM. *P < 0.05, **P < 0 .01, ***P < 0 .001 (compared with the control group).

with the green fluorescent protein (GFP) was inoculated intraperitoneally into female nude mice. After palpable tumors developed in approximately one week, MAP30 (250 μg/kg) was injected intraperitoneally into the tumor-bearing mice every other day for a total of 5 injections prior to sacrifice. Tumor-bearing mice treated with MAP30 exhibited significant suppression of tumor growth and an approximately 1.5-fold reduction in the number of tumor nodules compared to the control group (Fig. 4A, 4B & 4C). These findings indicate that MAP30 had potent *in vivo* efficacy against human ovarian cancer growth without any adverse effect on mouse body weight (Fig. 4D). Notably, similar ascites volumes were found in the MAP30 (250 μg/kg) treatment and control groups (Fig. 4E), which suggests alterations in the biological components of the ascites between the two groups. Therefore, GC-MS analysis of targeted metabolites in the ascites was performed, and the MAP30 treatment group exhibited a ~50% reduction in total fatty acid compared to the control group. Most fatty acids were unsaturated, such as C16:1, C18:1, C18:2, C22:1, C22:2, and C24:1, which serve the essential biosynthetic and bioenergetic needs of tumor cells (Fig. 4F & 4 G).

Although our study suggests that the MAP30 protein is non-toxic, the toxicity of this protein was examined in mouse models. Mice treated with a high dose of MAP30 (500 μg/kg) exhibited a ~10% weight loss (Fig. 4H & 4I). However, mice treated with lower doses of MAP30 (62.5 and 125 μg/kg) for more than one month did not show significant changes in body weight, and mortality was not observed Fig. 4H & 4I). Biochemical analysis revealed no observable changes in the levels of serum creatinine, blood urea nitrogen (BUN), alanine aminotransferase (ALT), aspartate aminotransferase (AST) or alkaline phosphatase in mice treated with 62.5 and 125 μg/kg MAP30 compared with the vehicle control group (Fig. 4J), which indicates no adverse effects on kidney and liver functions. A small deviation of AST was observed with a high dose of MAP30 (500 μg/kg) treatment, which suggests some minor liver damage (Fig. 4J). However, histopathology showed that the architecture of liver, kidney, and spleen in mice treated with low and high doses of MAP30 (62.5 and 500 μg/kg, respectively) looked similar to the control group (Fig. 4K), which demonstrates that MAP30 administration *in vivo* is devoid of severe toxic effects. However, some unforeseeable side effects may occur at a high dose of MAP30. Therefore, a study of the long-term toxicity of MAP30 in mice is warranted.

3.6. MAP30 synergistically enhances cisplatin-mediated cytotoxicity in vitro

Because MAP30 induced cell apoptosis and ferroptosis in ovarian cancer cells, we examined whether MAP30 sensitized ovarian cancer cells to cisplatin/taxol-induced cell cytotoxicity. Three advanced ovarian cancer cell lines were co-treated with cisplatin and/or MAP30 at different concentrations using a 2D culture system. Treatment with MAP30 alone or cisplatin alone inhibited the cell proliferation of ovarian cancer cells 50% and approximately 20%, respectively (Fig. 5A). However, co-treatment with MAP30 and cisplatin (0.5 μg/mL) enhanced the cell growth inhibition to at least 75% in ovarian cancer cells (Fig. 5A). Flow cytometry analysis indicated a significant and dose-dependent increase in the population of HEYA8 cells undergoing apoptotic death, and MAP30 dose-dependently increased cisplatin-mediated cell cytotoxicity by approximately 1.6- to 4.5-fold compared to the control (Fig. 5B).

Emerging evidence notes various restrictions of the 2D system in testing the chemoresistance of cancer cells, including its weak mimicking of the tumor microenvironment *in vivo* (22). An *in vitro* three-dimensional culture system (3D system) that recapitulates the *in vivo* tumor microenvironment and more accurately represents drug responses was developed recently (22). Therefore, we used the 3D culture system to further investigate whether MAP30 synergistically enhanced the cytotoxicity of cisplatin. The CellTiter-Glo® 3D cell viability assay was used to assess the sensitivity of 3D spheroid ovarian cancer cells cultured in a 2% Geltrex™ Matrix (Gibco BRL) to treatment with natural MAP30 and/or cisplatin. MAP30 or cisplatin treatment alone produced a dose-dependent inhibitory effect on the cell viability of OVCA433 (Fig. 5C) and HEY spheroids (Supplementary Fig. S4). We next determined whether co-treatment with MAP30 and cisplatin enhanced the therapeutic effect over each drug alone. Ovarian cancer cell lines, such as OVCA433 and HEY cells, were treated with serial concentrations of MAP30 and cisplatin in combination with a fixed molar ratio. The combination of both drugs remarkably induced a more significant slowing of cell viability than the respective treatments alone in OVCA433 (Fig. 5C) and HEY cells (Supplementary Fig. S4). The Combenefit algorithm was adopted to determine the effect of the drug combination, and the synergy matrix showed that dual inhibition generated an excellent synergistic anticancer effect on OVCA433 (Fig. 5D) and HEY cells (Supplementary Fig. S4). These data suggested that MAP30 synergistically enhanced cisplatin cell cytotoxicity in ovarian cancer cells.

3.7. MAP30 enhances cisplatin-induced cytotoxicity in vivo

To further investigate whether MAP30 enhanced cisplatin-induced cell cytotoxicity *in vivo*, ES2 tumor-bearing nude mice were injected intraperitoneally with MAP30 (125 μg/kg) and cisplatin (2 mg/kg) once every three days for a total of five injections prior to sacrifice. Consistent with the *in vitro* findings, co-treatment with MAP30 and cisplatin resulted in a remarkable tumor growth reduction, as evinced by a 4-fold lower tumor weight (Fig. 6A & 6B) and 2-fold fewer tumor nodules (Fig. 6A & 6C) compared to cisplatin treatment alone. The average ascites volumes were remarkably reduced with sole treatment of cisplatin or combined treatment of MAP30 and cisplatin (Fig. 6 D) without appreciably affecting the bodyweights of the mice at the end of the experiment (Fig. 6E). These findings confirmed that MAP30 was harmless *in vivo* and helped the inhibition of tumor growth via the enhancement of cisplatin-induced cytotoxicity.

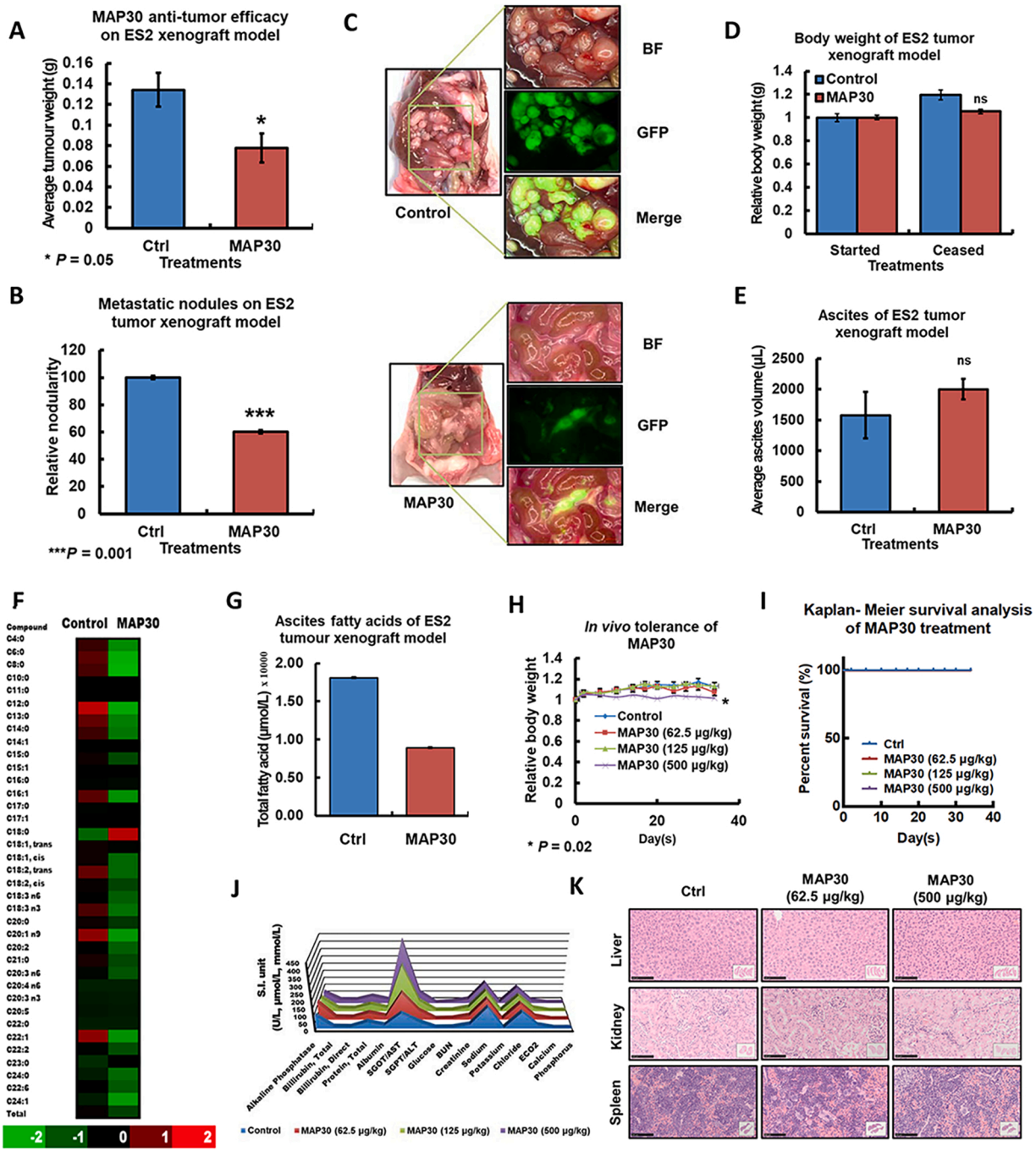

Fig. 4. MAP30 inhibits oncogenic properties of ovarian cancer cells solely. (A) A nude mouse tumor xenograft model showed that treatment with MAP30 by *i.p.* injection once every two days with a total of five doses. (A) Average tumor burden and (B) Relatively number of tumor nodules formed upon receiving MAP30 (250 μg/kg). (C) Fluorescence Stereomicroscopy directing the locations of tumor nodules in the peritoneal cavity of mice treated with or without MAP30 (250 μg/kg). BF = bright field. (D) MAP30 (250 μg/kg) exerted no significant reduction in the body weight of both groups of mice throughout the experiment. (E) MAP30 (250 μg/kg) used did not produce statistically significant variations in ascites of both groups of mice. (F) Metabolomics data plotted in a heat map showing the key differences in expression of 37 fatty acids between the ascites of control (Ctrl) and MAP30 (250 μg/kg) treated animals. (G) MAP30 (250 μg/kg) treatment reduced the total fatty acid in the ascites of the ES2 xenograft mouse tumor model compared with the untreated control. (H) MAP30 (62.5, 125, and 500 μg/kg) exerted no noticeable reduction on the bodyweight of all groups of mice throughout the experiment. (I) Kaplan-Meier survival analysis showed no significant differences in survival curves between the low dose of MAP30. (J) Biochemical tests showed low doses of MAP30 exhibited no significant adverse effect on liver and kidney functions as controls. (K) Hematoxylin and Eosin (H&E) staining showed histopathology of liver, kidney, and spleen of control and MAP30-treated groups (Ctrl, 62.5 μg/kg, and 500 μg/kg). (Sale bar = 100μm) All bar charts are expressed as mean ± SEM. *P < 0.05, **P < 0 .01, ***P < 0 .001 (compared with the control group). ns = No Significance.

3.8. MAP30 suppresses glycolysis and de novo lipogenesis in ovarian cancer cells

Mounting evidence suggests that AMPK is a metabolic tumor suppressor that controls tumor development and progression (23). The present study investigated whether MAP30 altered tumor metabolism to achieve its suppressive effects on ovarian cancer oncogenic properties. L-lactate assay analysis showed that ovarian cancer cells generally produced a relatively higher lactate level than immortalized human ovarian surface epithelial control cells throughout the two-day culture

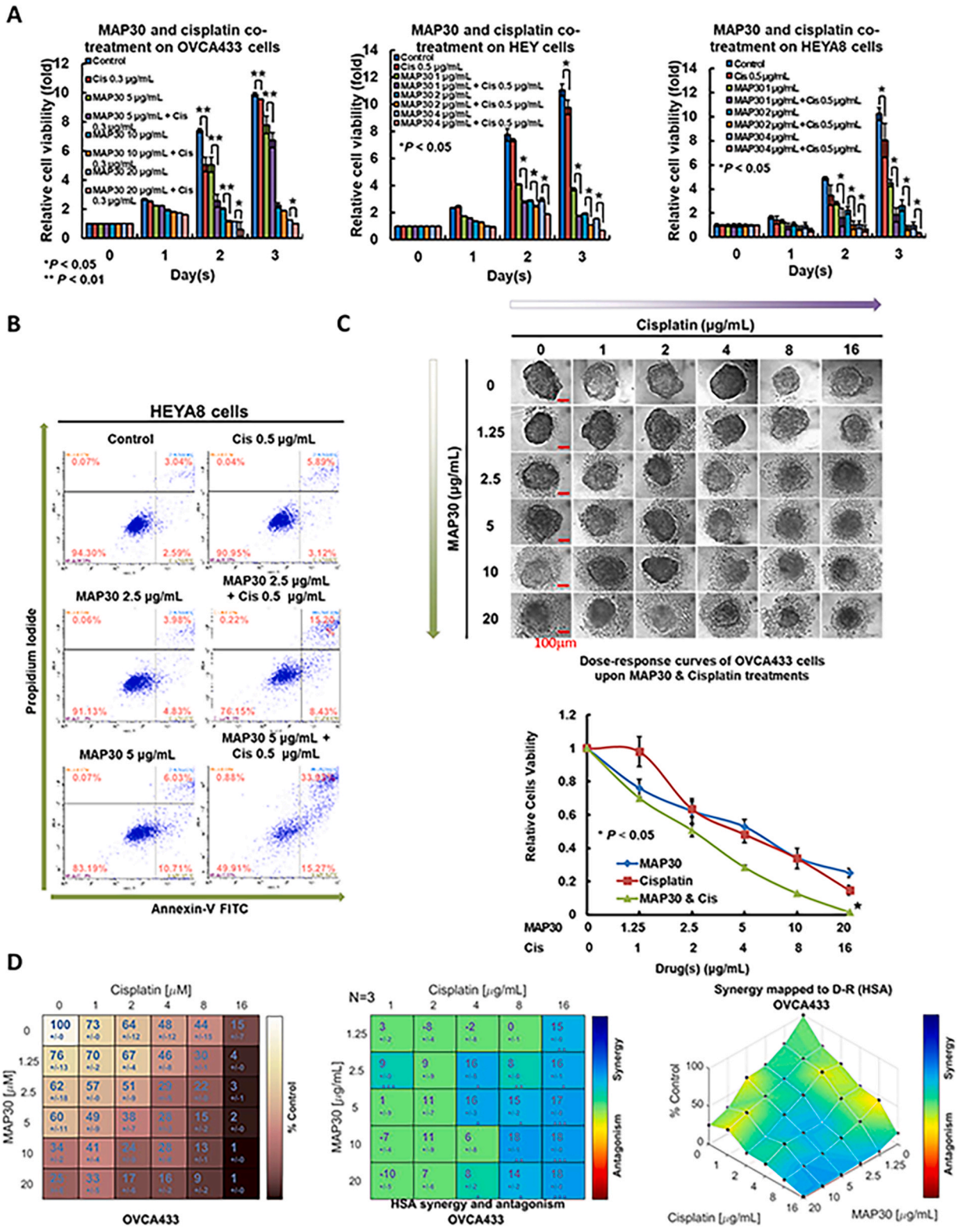

Fig. 5. MAP30 synergistically enhances cisplatin-mediated cytotoxicity in ovarian cancer cells. (A) XTT cell proliferation assay demonstrated that the growth rates of OVCA433, HEY, and HEYA8 cells were significantly reduced to the greatest extent by MAP30 combined with cisplatin. In OVC433 cells, MAP30 (5-20 μg/mL) combined with cisplatin (0.3 μg/mL) were used, while in both HEY and HEYA8 cells, MAP30 (1-4 μg/mL) combined with cisplatin (0.5μg/mL) were used. (B) Flow cytometry analysis of Annexin-V and Propidium Iodide (PI) staining of apoptotic cells revealed a dose-dependent increase in the population of apoptotic cells following treatment with MAP30, and the increase was more apparent when cells were co-treated with MAP30 (2.5 and 5 μg/mL) and cisplatin (0.5 μg/mL) or 48 h. (C) Morphological examination of OVCA433 cells treated with increasing concentrations of MAP30 and/or cisplatin for 3 days (*upper*). (Scale bar = 100 μm). The **c**ell **v**iability of OVCA433 cells treated with increasing concentrations of MAP30 and/ or cisplatin for 3 days with the determination of IC50 (*lower*). (D) Matrix representation showing the percentage of viable cells after treatment with increasing concentrations of MAP30 and/or cisplatin for 3 days (*left*). Synergy matrix (*middle*) and surface plots (*right*) showing the synergistic effect between cisplatin and MAP30 on OVCA433 cells (N = 3). All bar or line charts are expressed as mean + SEM. *P < 0.05, **P < 0 .01, ***P < 0 .001 (compared with the control group).

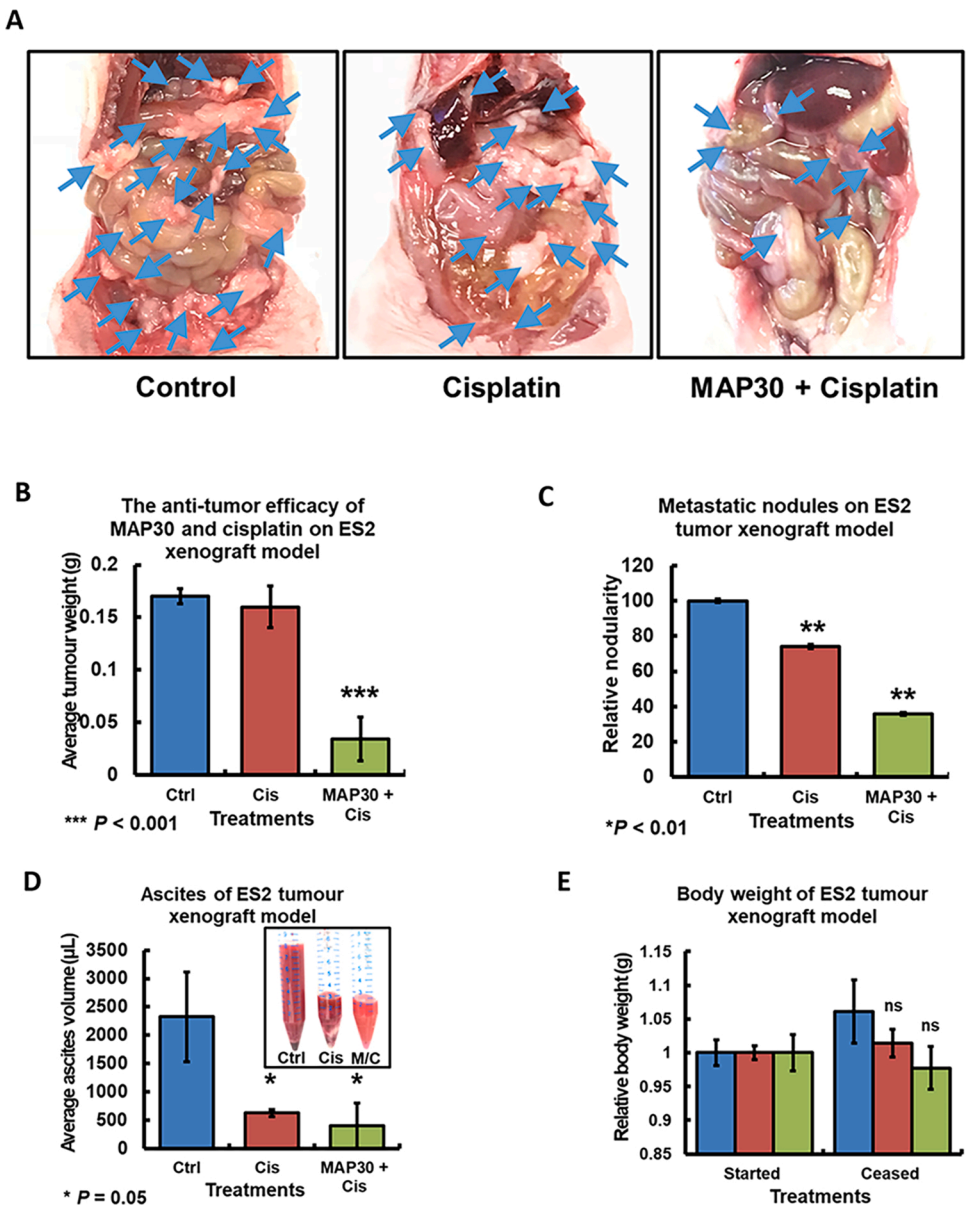

Fig. 6. MAP30 enhances cisplatin-mediated tumor growth *in vivo*. To establish a nude mouse tumor xenograft model, ES2 cells were intraperitoneally inoculated into 4-5 weeks old female nude mice. About one week after injection of tumor cells, treatment with MAP30 (125 μg/kg) and cisplatin (2 mg/kg) were initiated and carried out every other day with a total of five injections. (A) Representative photographs of peritoneal dissemination with arrows (Blue) directing the locations of tumor nodules in the peritoneal cavity of mice treated vehicle PBS (Ctrl), cisplatin (2 mg/kg) as well as MAP30 (125 μg/kg) and cisplatin (2 mg/kg). (B) Average tumor burden and (C) relatively number of tumor nodules formed upon co-treatment were much lower than the cisplatin alone and the vehicle-treated control. (D) Co-treatment of MAP30 and cisplatin or cisplatin alone exerted a significant reduction in the ascites of both groups of mice when compared with vehicle-treated control. (E) Co-treatment of MAP30 and cisplatin alone exerted no substantial reduction in the bodyweight of both groups of mice. All bar charts are expressed as mean + SEM. *P < 0.05, **P < 0 .01, ***P < 0 .001 (compared with the control group).

(Fig. 7A). This enhanced lactate production in ovarian cancer cells was significantly counteracted by treatment with the natural AMPK activator MAP30 (40 μg/mL) and the positive controls using pharmaceutical AMPK activators such as AICAR (1 mM) and A23187 (2 μM) (Fig. 7B), which indicates that the reduction in glycolysis in ovarian cancer cells occurred via MAP30-mediated AMPK activation. Notably, the reduced glycolysis positively correlated with a decrease in the activities of glycolytic enzymes, such as hexokinase and LDH, which were significantly suppressed by 30-80% and 50-90%, respectively, following MAP30 (10-40 μg/mL) treatment for 24 to 48 h (Fig. 7C and 7D). Notably, we hypothesized that the net reduction of glycolysis via MAP30-mediated AMPK activation was attributed to a decline in carbon flux. Therefore, a glucose uptake assay was performed. MAP30 (10-40 μg/mL) behaved similarly to the pharmaceutical AMPK activator AICAR (1 mM) and inhibited glucose uptake in OVCA433 cells by ~30% to 60% in a dose-dependent manner (Fig. 7E). Western blot analysis further confirmed the remarkable reduction of the expression of GLUT1 and GLUT3 glucose transporters following MAP30 (40 μg/mL) treatment in a time-dependent manner, but another glucose transporter, GLUT4, remained unchanged (Fig. 7F). These data indicate that MAP30 inhibits glucose uptake via a reduction in GLUT-1 and -3 transporters.

The omentum is a preferential site of ovarian cancer metastasis (24–26). Therefore, we hypothesized that free fatty acids enriched in the omental microenvironment specifically modulated ovarian tumor cells to promote malignant cell survival and metastatic cancer cell dissemination. The OCM-cultured ovarian cancer cell line OVCA433 showed an increase of lipid droplet formation using Nile Red fluorescent staining, and MAP30 co-treatment (5 and 10 μg/mL) reduced the number of lipid droplets 50-70% (Fig. 7G). To further determine whether MAP30 accelerated catabolic lipolysis within human ovarian cancer cells, a lipolysis assay was performed. The results showed that MAP30 (10 and 40 μg/mL) induced an approximately 2-4 fold increase in cellular lipolysis in ovarian cancer cells (Fig. 7H). The ATP detection assay revealed a significant reduction in ATP production as a result of MAP30 (10 and 40 μg/mL) treatment in ovarian cancer cells (Fig. 7I). Collectively, our findings showed that MAP30 interrupted glucose uptake and lipid droplet formation in ovarian cancer cells, which suggests that MAP30 would inhibit ovarian cancer aggressiveness and metastasis in the ascites microenvironment.

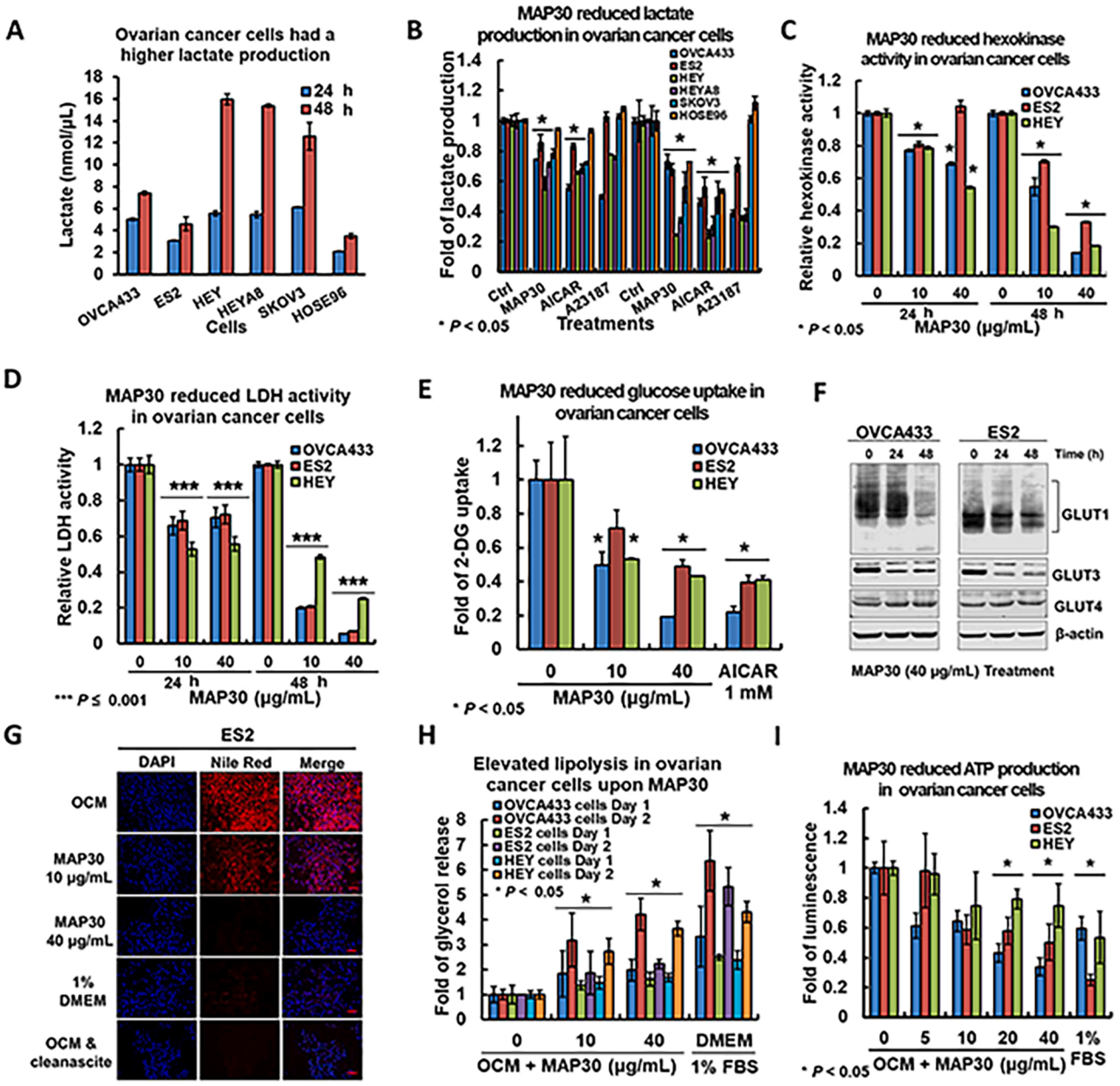

Fig. 7. MAP30 alters glycolysis and lipid metabolism in ovarian cancer cells. (A) Ovarian cancer cells exhibited augmented aerobic glycolysis, as evidenced by the higher lactate production after 24 and 48 h of culture when compared with HOSE 96-9-18 cells. (B) Treatment of MAP30 (40 μg/mL) for 24 h (*left*) and 48 h (*right*) significantly reduced lactate production in ovarian cancer cells. AICAR (1 mM) and A23187 (2 μM) were used as positive controls of AMPK activation. (C) Hexokinase activity and (D) lactate dehydrogenase (LDH) activities were diminished by MAP30 (10 to 40 μg/mL) time- and dose-dependently. (E) Glucose uptake assay showed that glucose uptake in ovarian cancer cells declined after MAP30 (10 to 40 μg/mL) treatment with AICAR (1 mM) as the positive control. (F) Western blot analysis showed the expressions of GLUT1 and GLUT3 were reduced, while GLUT4 remained unchanged in ovarian cancer cells after MAP30 (40 μg/mL) for 24 to 48 h. (G) Nile Red fluorescence of lipid-loaded ES2 in OCM culture for 48 h. The 1%DMEM and OCM with Cleanascite treatment were used as negative controls. (H) Before OCM and MAP30 treatments, ovarian cancer cells were starved in DMEM without FBS overnight, and subsequent cellular lipolysis was measured by the lipolysis assay. The finding showed an increase in lipolysis of ovarian cancer cells upon MAP30 (10 and 40 μg/mL) treatment for 24 to 48 h with 1% FBS DMEM as the positive control. (I) MAP30 (10 and 40 μg/mL) treatment for 48 h reduced ATP production in ovarian cancer cells.

4. Discussion

TCM targets cancer cells and treats the entire body, including the Qi, blood, organs, and the immune system (27). TCM is used as complementary alternative medicine. The bioactive compounds from TCM possess noticeable anticancer activity via regulation of multiple levels and targets in cancer cells (28). Therefore, TCM and its bioactive compounds may be useful in modern cancer therapy as ideal adjuvants. Bitter melon or bitter gourd has been in medicinal use in China and India for improving digestion and the treatment of diabetes and obesity, and it is known for its "plant insulin" activity (29,30). We previously reported that the extract of bitter melon (BME) exerted a suppressive effect on ovarian cancer cells via activation of AMPK/mTOR signaling (11). The present study isolated MAP30 protein from the dried bitter melon seeds. Our functional and biochemical analyses suggest that MAP30 is a major bioactive component in BME.

BME contains various bioactive compounds, and it showed anticancer effects in various human cancers (31–33). For example, kuguacin J (KJ) isolated from bitter melon extract reduced the resistance of ovarian cancer cells to paclitaxel (31). The ribonuclease RNase MC2

induced apoptotic mediators and cell apoptosis in human breast cancer (33). A novel peptide from bitter melon, BG-4, promoted cell apoptosis in human colon cancer (32). However, these studies did not show any relationship or function of AMPK. Bitter melon has been used in China and India for curing diabetes because it serves the same purpose as metformin, which is used in the first-line treatment of diabetes (34). This activity suggests that bitter melon possesses a functional effect on AMPK activation. The seeds of bitter melon are used in Chinese folk medicine for the treatment of diabetes and obesity (30). This use may be due to the enriched bioactive metabolites in bitter melon seeds that modulate cell metabolism, which was found in a recent study using metabolomics profiling (35). Fang et al. reported that the MAP30 protein isolated from bitter melon dried seeds promoted cell apoptosis in prostate cancer (36). This result urged us to separate the MAP30 protein from dried bitter melon seeds. The yield of MAP30 protein was 40 mg per 100 g of bitter melon seeds. Notably, we demonstrated that MAP30 was a main component of BME. MAP30 activated AMPK via the CaMKKβ pathway in an AMP-independent manner and suppressed mTOR and the novel AKT/ERK/FOXM1 signaling pathways to produce suppressive effects on ovarian cancer.

AMPK is a key energy sensor in healthy cells and a crucial factor for tumor development (37), by maintaining the cellular energy balance that regulates multiple cellular metabolic pathways (38). Emerging evidence showed that malignant cells required high AMPK activity to initially overcome the metabolic stress from the tumor microenvironment, but relatively lower AMPK activity was favored in advanced cancers to enhance cell growth and progression (39). These data indicate that advanced and more aggressive ovarian cancer cells prefer low AMPK activity to reduce metabolic constraints, e.g., mTOR to exert high oncogenic properties. These data also provide advantages for AMPK activators in impairing ovarian cancer cell functions selectively without affecting normal cells. Natural MAP30 isolated from non-toxic bitter melon increased AMPK activity via the CaMKKβ pathway and in an AMP-independent manner, which provides another angle to target cancer cells whose survival and other cellular activities are not affected by an AMP-stressed condition, such as a nutrient-enriched microenvironment. Our study showed that natural MAP30 significantly suppressed cell growth via S-phase cell cycle arrest, cell migration/invasion, and tumor growth or colonization in a mouse tumor xenograft model. mTOR signaling is an essential pathway in cell metabolism, growth, proliferation, survival, and drug resistance (40). However, mTOR inhibitors, such as rapamycin, temsirolimus (CCI-779), everolimus (RAD001), and ridaforolimus (AP23573), do not exhibit broad and potent anticancer and anti-chemoresistance effects (41). On the other hand, our findings suggest that MAP30 didn't show this deficiency in impairing ovarian cancer cell functions.

Emerging evidence suggests that the ascites microenvironment provides growth factors and reprograms cancer cell metabolism to promote ovarian cancer progression via peritoneal metastases (42). Therefore, the targeting of cancer cell metabolism is a promising method to impair ovarian cancer aggressiveness in the tumor microenvironment (42). Our findings indicated that MAP30 inhibited oncogenic AKT/ERK/FOXM1 signaling cascades and modulated cell metabolism, such as reducing glucose uptake via suppression of the major glucose transporters GLUT1 and GLUT3 expression, lipid droplet formation, and even lipolysis. The suppression of glycolysis and lipid metabolism led to a significant reduction in tumor dissemination in our murine ovarian cancer model. Our findings demonstrated that MAP30 activated the AMPK pathway via CaMKKβ, which led to a Ca^{2+} increase in ovarian cancer cells. Unrestrained Ca^{2+} signals may produce mitochondrial damage and increase ROS stress (43,44). The excess ROS induces caspase-dependent apoptotic cell death pathway activation in ovarian cancer cells.

In addition to mediating caspase activation and cell apoptosis, the excess of ROS may induce lipid peroxidation at cell membranes and lead to iron-dependent cell death, i.e., ferroptosis (20). Our previous study showed that ovarian cancer cells take up free fatty acids (FFAs) from the ascites microenvironment to support their metastatic progression in peritoneal metastases (42). These metastatic ovarian cancer cells generally possess a higher ratio of unsaturated FFAs to saturated FFAs in the ascites microenvironment (42). Because polyunsaturated fatty acids (PUFAs) are excellent substrates for lipid peroxidation and are increased in metastatic ovarian cancer cells (45), we investigated whether MAP30 induced ferroptosis to inhibit metastatic colonization in ovarian cancer. Erastin is a synthetic lethal compound that triggers ferroptosis in cancer cells via xCT/GPX4 and GSH depletion. We used Erastin as the positive control (21) and found that MAP30 similarly suppressed GPX4, reduced the GSH/GSSG ratio, and increased the amount of ROS, which enhanced lipid peroxidation (20). However, ferrostatin-1 (Fer-1) prevented the induction of lipid peroxidation, which confirmed that MAP30 was an inducer of ferroptosis in ovarian cancer cells. Erastin is a Class 1 ferroptosis inducer (FIN) that induces ferroptosis via the inactivation of GPX and depletion of intracellular GSH (46). Similar to Erastin, the depletion of intracellular antioxidant systems by MAP30 led to the accumulation of lipid peroxides, which enhanced the susceptibility of ovarian cancer cell-free radical oxidative damage and cell death. Given that MAP30 is a natural AMPK activator, it is of interest to investigate whether AMPK activity is involved in ferroptosis. In fact, several recent studies showed AMPK activity mediated ferroptosis, but the outcomes in different cell types remain controversial. For instance, Xong X. *et al.* demonstrated that AMPK phosphorylated BECN1, which blocked system xCT and enhanced ferroptosis via an Erastin-type induction in colon adenocarcinoma cells (47). In contrast, Lee H. *et al.* showed that stress-activated AMPK inhibited ferroptosis in ischemic tissues via an RSL3-driven induction (48). In this study, we found that the depletion of AMPK reduced MAP30-induced Ca^{2+} influx and ROS but caused less reduction of GSH/GSSG ratio and lipid peroxidation in ovarian cancer cells. These results indicate that the presence or absence of AMPK has a certain influence on MAP30-induced ferroptosis in ovarian cancer cells, but the intimate mechanisms remain to be elucidated.

5. Conclusion

MAP30 is a natural AMPK activator and regulates multiple levels and targets simultaneously. Notably, these activities of MAP30 enhance its anticancer response and anti-chemoresistance in ovarian cancers, which supports its use as a supplement to synergistically improve the efficacy of current chemotherapy regimes in advanced ovarian cancers.

Author contributions

DC, MY and HN designed research; DC, MY, YC and YX performed the experiments; DC, HY, DX, JZ, KC, TN and HN contributed new reagents-analytic tools; DC, MY, YC, YX, TN and HN analyzed and interpreted data; DC, MY and TN wrote and edited the manuscript; DC and HN study supervision. All authors had the final approval of the submitted and published versions.

Declaration of Competing Interest

The Authors declare no Competing Financial or Non-Financial Interests.

Patent

A Chinese patent application number CN202010143127.4 was filed on 4 March 2020, and a PCT application number PCT/CN2020/109639 was filed on 17 August 2020.

Financial Statement

This study was supported by the Health and Medical Research Fund - Full Grant, Hong Kong (13142271).

Acknowledgments

We would like to thank by Prof. AWS Wong, School of Biological Sciences, HKU, for providing HEY and HEYA8 cells, Prof. George SW Tsao, School of Biomedical Sciences, HKU, for providing OVCA433, SKOV3, and HOSEs cells, Prof. JB Zhan, Zhejiang University, PR China for providing recombinant MAP30, and Prof. DG Hardie, Dundee University, UK. for providing pL-CRISPR.EFS.GFP plasmids for AMPK α1 and α2 CRISPR/Cas9 gene knockout, and a pair of WT and R531G AMPKγ2 isogenic HEK293 cells, and the assistance of The University of Hong Kong Li Ka Shing Faculty of Medicine Centre for PanorOmic Sciences Proteomics and Metabolomics Core for Gas Chromatography-Mass Spectrometry (GC-MS) analysis of targeted metabolites in murine ascites.

Human ethics: The Institutional Review Board of the University of Hong Kong/Hospital Authority Hong Kong West Cluster (HKU/HA HKW IRS) (IRS Reference Number: UW 11-298)- For the collection and use of human omental tissues from surgeries performed at Queen Mary Hospital, Hong Kong SAR, P.R.China.

Animal ethics: The Committee on the Use of Live Animals in Teaching and Research of The University of Hong Kong (CULATR number: 3817-15).

Appendix A. Supplementary data

Supplementary material related to this article can be found, in the online version, at doi:https://doi.org/10.1016/j.phrs.2020.105157.

References

[1] H.K. Park, J.J. Ruterbusch, M.L. Cote, Recent Trends in Ovarian Cancer Incidence and Relative Survival in the United States by Race/Ethnicity and Histologic Subtypes, Cancer epidemiology, biomarkers & prevention: a publication of the American Association for Cancer Research, cosponsored by the American Society of Preventive Oncology 26 (10) (2017) 1511–1518.
[2] J. van Baal, C.J.F. van Noorden, R. Nieuwland, K.K. Van de Vijver, A. Sturk, W. J. van Driel, G.G. Kenter, C.A.R. Lok, Development of Peritoneal Carcinomatosis in Epithelial Ovarian Cancer: A Review, J Histochem Cytochem. 66 (2) (2018) 67–83.
[3] E.L. Christie, D.D.L. Bowtell, Acquired chemotherapy resistance in ovarian cancer, Ann Oncol. 28 (suppl_8) (2017) viii13–viii15.
[4] B.B. Kahn, T. Alquier, D. Carling, D.G. Hardie, AMP-activated protein kinase: ancient energy gauge provides clues to modern understanding of metabolism, Cell Metab. 1 (1) (2005) 15–25.
[5] H.T. Kwan, D.W. Chan, P.C. Cai, C.S. Mak, M.M. Yung, T.H. Leung, O.G. Wong, A. N. Cheung, H.Y. Ngan, AMPK activators suppress cervical cancer cell growth through inhibition of DVL3 mediated Wnt/beta-catenin signaling activity, PLoS One. 8 (1) (2013) e53597.
[6] Y. Yi, L. Gao, M. Wu, J. Ao, C. Zhang, X. Wang, M. Lin, J. Bergholz, Y. Zhang, Z. J. Xiao, Metformin Sensitizes Leukemia Cells to Vincristine via Activation of AMP-activated Protein Kinase, Journal of Cancer. 8 (13) (2017) 2636–2642.
[7] M. Daugan, A. Dufay Wojcicki, B. d'Hayer, V. Boudy, Metformin: An anti-diabetic drug to fight cancer, Pharmacological research 113 (Pt A) (2016) 675–685.
[8] S. Wang, S. Long, W. Wu, Application of Traditional Chinese Medicines as Personalized Therapy in Human Cancers, The American journal of Chinese medicine 46 (5) (2018) 953–970.
[9] Z. Yan, Z. Lai, J. Lin, Anticancer Properties of Traditional Chinese Medicine, Combinatorial chemistry & high throughput screening 20 (5) (2017) 423–429.
[10] E.F. Fang, T.B. Ng, Bitter gourd (Momordica charantia) is a cornucopia of health: a review of its credited antidiabetic, anti-HIV, and antitumor properties, Current molecular medicine. 11 (5) (2011) 417–436.
[11] M.M. Yung, F.A. Ross, D.G. Hardie, T.H. Leung, J. Zhan, H.Y. Ngan, D.W. Chan, Bitter Melon (Momordica charantia) Extract Inhibits Tumorigenicity and Overcomes Cisplatin-Resistance in Ovarian Cancer Cells Through Targeting AMPK Signaling Cascade, Integr Cancer Ther. 15 (3) (2016) 376–389.
[12] A.S. Bourinbaiar, S. Lee-Huang, Potentiation of anti-HIV activity of anti-inflammatory drugs, dexamethasone and indomethacin, by MAP30, the antiviral agent from bitter melon, Biochemical and biophysical research communications. 208 (2) (1995) 779–785.
[13] A.M. Martinez, J. Mirkovic, Z.A. Stanisz, F.S. Patwari, W.S. Yang, NSC-34 motor neuron-like cells are sensitized to ferroptosis upon differentiation, FEBS Open Bio. 9 (4) (2019) 582–593.
[14] G.Y. Di Veroli, C. Fornari, D. Wang, S. Mollard, J.L. Bramhall, F.M. Richards, D. I. Jodrell, Combenefit: an interactive platform for the analysis and visualization of drug combinations, Bioinformatics 32 (18) (2016) 2866–2868.
[15] J.N. Kuznetsov, G.J. Leclerc, G.M. Leclerc, J.C. Barredo, AMPK and Akt determine apoptotic cell death following perturbations of one-carbon metabolism by regulating ER stress in acute lymphoblastic leukemia, Mol Cancer Ther. 10 (3) (2011) 437–447.
[16] M.M. Yung, D.W. Chan, V.W. Liu, K.M. Yao, H.Y. Ngan, Activation of AMPK inhibits cervical cancer cell growth through AKT/FOXO3a/FOXM1 signaling cascade, BMC cancer. 13 (1) (2013) 327.
[17] P. Maher, K. van Leyen, P.N. Dey, B. Honrath, A. Dolga, A. Methner, The role of Ca (2+) in cell death caused by oxidative glutamate toxicity and ferroptosis, Cell Calcium. 70 (2018) 47–55.
[18] L.J. Su, J.H. Zhang, H. Gomez, R. Murugan, X. Hong, D. Xu, F. Jiang, Z.Y. Peng, Reactive Oxygen Species-Induced Lipid Peroxidation in Apoptosis, Autophagy, and Ferroptosis, Oxid Med Cell Longev. 2019 (2019) 5080843.
[19] C. Gaucher, A. Boudier, J. Bonetti, I. Clarot, P. Leroy, M. Parent, Glutathione: Antioxidant Properties Dedicated to Nanotechnologies, Antioxidants (Basel). 7 (5) (2018).
[20] Y. Shibata, H. Yasui, K. Higashikawa, N. Miyamoto, Kuge Y. Erastin, a ferroptosis-inducing agent, sensitized cancer cells to X-ray irradiation via glutathione starvation in vitro and in vivo, PLoS One. 14 (12) (2019) e0225931.
[21] S. Hao, J. Yu, W. He, Q. Huang, Y. Zhao, B. Liang, S. Zhang, Z. Wen, S. Dong, J. Rao, W. Liao, M. Shi, Cysteine Dioxygenase 1 Mediates Erastin-Induced Ferroptosis in Human Gastric Cancer Cells, Neoplasia. 19 (12) (2017) 1022–1032.
[22] K. Dzobo, A. Rowe, D.A. Senthebane, M.A.M. AlMazyadi, V. Patten, M.I. Parker, Three-Dimensional Organoids in Cancer Research: The Search for the Holy Grail of Preclinical Cancer Modeling, OMICS. 22 (12) (2018) 733–748.
[23] B. Faubert, G. Boily, S. Izreig, T. Griss, B. Samborska, Z. Dong, F. Dupuy, C. Chambers, B.J. Fuerth, B. Viollet, O.A. Mamer, D. Avizonis, R.J. DeBerardinis, P. M. Siegel, R.G. Jones, AMPK is a negative regulator of the Warburg effect and suppresses tumor growth in vivo, Cell Metab. 17 (1) (2013) 113–124.
[24] L.E. Drake, K.F. Macleod, Tumour suppressor gene function in carcinoma-associated fibroblasts: from tumour cells via EMT and back again? J Pathol. 232 (3) (2014) 283–288.
[25] D.F. Quail, J.A. Joyce, Microenvironmental regulation of tumor progression and metastasis, Nature medicine. 19 (11) (2013) 1423–1437.
[26] A. Nowicka, F.C. Marini, T.N. Solley, P.B. Elizondo, Y. Zhang, H.J. Sharp, R. Broaddus, M. Kolonin, S.C. Mok, M.S. Thompson, W.A. Woodward, K. Lu, B. Salimian, D. Nagrath, A.H. Klopp, Human omental-derived adipose stem cells increase ovarian cancer proliferation, migration, and chemoresistance, PLoS One. 8 (12) (2013) e81859.
[27] S. Xutian, J. Zhang, W. Louise, New exploration and understanding of traditional Chinese medicine, The American journal of Chinese medicine 37 (3) (2009) 411–426.
[28] C.Y. Wang, X.Y. Bai, C.Y.H. Wang, Traditional Chinese medicine: a treasured natural resource of anticancer drug research and development, The American journal of Chinese medicine 42 (3) (2014) 543–559.
[29] M.A. Alam, R. Uddin, N. Subhan, M.M. Rahman, P. Jain, H.M. Reza, Beneficial role of bitter melon supplementation in obesity and related complications in metabolic syndrome, J Lipids. 2015 (2015) 496169.
[30] J. Yin, H. Zhang, J. Ye, Traditional chinese medicine in treatment of metabolic syndrome, Endocr Metab Immune Disord Drug Targets. 8 (2) (2008) 99–111.
[31] P. Pitchakarn, S. Umsumarng, S. Mapoung, P. Ting, P. Temviriyanukul, W. Punfa, W. Pompimon, P. Limtrakul, Kuguacin J isolated from bitter melon leaves modulates paclitaxel sensitivity in drug-resistant human ovarian cancer cells, Journal of natural medicines 71 (4) (2017) 693–702.
[32] V.P. Dia, H.B. Krishnan, BG-4, a novel anticancer peptide from bitter gourd (Momordica charantia), promotes apoptosis in human colon cancer cells, Scientific reports. 6 (2016) 33532.
[33] E.F. Fang, C.Z. Zhang, W.P. Fong, T.B. Ng, RNase MC2: a new Momordica charantia ribonuclease that induces apoptosis in breast cancer cells associated with activation of MAPKs and induction of caspase pathways, Apoptosis: an international journal on programmed cell death 17 (4) (2012) 377–387.
[34] E. Basch, S. Gabardi, C. Ulbricht, Bitter melon (Momordica charantia): a review of efficacy and safety, American journal of health-system pharmacy: AJHP: official journal of the American Society of Health-System Pharmacists. 60 (4) (2003) 356–359.
[35] S. Zhou, P.M. Allard, C. Wolfrum, C. Ke, C. Tang, Y. Ye, J.L. Wolfender, Identification of chemotypes in bitter melon by metabolomics: a plant with potential benefit for management of diabetes in traditional Chinese medicine, Metabolomics. 15 (8) (2019) 104.
[36] E.F. Fang, C.Z. Zhang, J.H. Wong, J.Y. Shen, C.H. Li, T.B. Ng, The MAP30 protein from bitter gourd (Momordica charantia) seeds promotes apoptosis in liver cancer cells in vitro and in vivo, Cancer Lett. 324 (1) (2012) 66–74.
[37] M.M. Yung, H.Y. Ngan, D.W. Chan, Targeting AMPK signaling in combating ovarian cancers: opportunities and challenges, Acta Biochim Biophys Sin (Shanghai). 48 (4) (2016) 301–317.
[38] D.G. Hardie, S.C. Lin, AMP-activated protein kinase - not just an energy sensor, F1000Research. 6 (2017) 1724.
[39] C. Li, V.W. Liu, P.M. Chiu, K.M. Yao, H.Y. Ngan, D.W. Chan, Reduced expression of AMPK-beta1 during tumor progression enhances the oncogenic capacity of advanced ovarian cancer, Mol Cancer. 13 (2014) 49.
[40] Y. Guri, M.N. Hall, mTOR Signaling Confers Resistance to Targeted Cancer Drugs, Trends in cancer. 2 (11) (2016) 688–697.
[41] H. Populo, J.M. Lopes, P. Soares, The mTOR signalling pathway in human cancer, International journal of molecular sciences 13 (2) (2012) 1886–1918.
[42] R.R. Chen, M.M.H. Yung, Y. Xuan, S. Zhan, L.L. Leung, R.R. Liang, T.H.Y. Leung, H. Yang, D. Xu, R. Sharma, K.K.L. Chan, S.F. Ngu, H.Y.S. Ngan, D.W. Chan, Targeting of lipid metabolism with a metabolic inhibitor cocktail eradicates peritoneal metastases in ovarian cancer cells, Commun Biol. 2 (2019) 281.

[43] A. Gorlach, K. Bertram, S. Hudecova, O. Krizanova, Calcium and ROS: A mutual interplay, Redox Biol. 6 (2015) 260–271.
[44] M. Carraro, P. Bernardi, Calcium and reactive oxygen species in regulation of the mitochondrial permeability transition and of programmed cell death in yeast, Cell Calcium. 60 (2) (2016) 102–107.
[45] M.S. Shchepinov, Polyunsaturated Fatty Acid Deuteration against Neurodegeneration, Trends Pharmacol Sci. 41 (4) (2020) 236–248.
[46] W.S. Yang, R. SriRamaratnam, M.E. Welsch, K. Shimada, R. Skouta, V. S. Viswanathan, J.H. Cheah, P.A. Clemons, A.F. Shamji, C.B. Clish, L.M. Brown, A. W. Girotti, V.W. Cornish, S.L. Schreiber, B.R. Stockwell, Regulation of ferroptotic cancer cell death by GPX4, Cell. 156 (1-2) (2014) 317–331.
[47] X. Song, S. Zhu, P. Chen, W. Hou, Q. Wen, J. Liu, Y. Xie, J. Liu, D.J. Klionsky, G. Kroemer, M.T. Lotze, H.J. Zeh, R. Kang, D. Tang, AMPK-Mediated BECN1 Phosphorylation Promotes Ferroptosis by Directly Blocking System Xc(-) Activity, Curr Biol. 28 (15) (2018) 2388–2399, e2385.
[48] H. Lee, F. Zandkarimi, Y. Zhang, J.K. Meena, J. Kim, L. Zhuang, S. Tyagi, L. Ma, T. F. Westbrook, G.R. Steinberg, D. Nakada, B.R. Stockwell, B. Gan, Energy-stress-mediated AMPK activation inhibits ferroptosis, Nat Cell Biol. 22 (2) (2020) 225–234.